Applied Physics Letters ARTICLE scitation.org/journal/apl

Hybrid bilayer plasmonic metasurfaces with intrinsic chiral optical responses

Cite as: Appl. Phys. Lett. **122**, 181702 (2023); doi: 10.1063/5.0147417
Submitted: 22 February 2023 · Accepted: 24 April 2023 ·
Published Online: 4 May 2023

Zhancheng Li,[1] Yifan Jiang,[1] Wenwei Liu,[1] Yuebian Zhang,[1,a)] Hua Cheng,[1,a)] Junjie Li,[2] Jianguo Tian,[1] and Shuqi Chen[1,3,a)]

AFFILIATIONS

[1]The Key Laboratory of Weak Light Nonlinear Photonics, Ministry of Education, Smart Sensing Interdisciplinary Science Center, Renewable Energy Conversion and Storage Center, School of Physics and TEDA Institute of Applied Physics, Nankai University, Tianjin 300071, China

[2]Beijing National Laboratory for Condensed Matter Physics, Institute of Physics, Chinese Academy of Sciences, Beijing 100190, China

[3]The Collaborative Innovation Center of Extreme Optics, Shanxi University, Taiyuan, Shanxi 030006, China

[a)]**Authors to whom correspondence should be addressed:** ybzhang@nankai.edu.cn; hcheng@nankai.edu.cn; and schen@nankai.edu.cn

ABSTRACT

Plasmonic metasurfaces with giant chiral optical responses are good candidates for chirality study and application, which are usually composed of few-layer or three-dimensional nanostructures. Here, we demonstrate that hybrid bilayer plasmonic metasurfaces simply fabricated via a facile one-step nanofabrication process are good candidates for the realization of intrinsic chiral optical responses and spin-selective transmission. We prove that the intrinsic chiral optical response of the proposed metasurface, which can be easily manipulated, is attributed to the spin-selective collective interference of locally enhanced electric fields caused by the strong interlayer coupling. We further experimentally prove the advantages of fabricated hybrid bilayer plasmonic metasurfaces for optical encryption. With the advantages of compact design, chiral optical response easy to control and lower fabrication demand, the proposed metasurfaces can further expand the applications of chiral plasmonic nanostructures in the area of spin nanophotonics, nonlinear optics, and optical sensing.

Chirality is a geometrical quality of objects, describing objects that cannot be superposed onto their mirror images. Chirality is ubiquitous in our daily life; it is not only a signature of molecules but also a prerequisite for some biological and chemical processes.[1–3] Circular birefringence and circular dichroism are two chiral optical responses when chiral objects interact with optical waves. Circular dichroism, which is defined as the difference in absorbance for left-handed circularly polarized (LCP) waves and right-handed circularly polarized (RCP) waves, serves as the main mean for the detection and discrimination of chiral enantiomorphs. However, due to the small size of natural molecules compared with the wavelength of optical waves, the chiral optical responses in natural molecules are quite subtle. The detection and discrimination of chirality and the study of its origin remain challenges.

Recently, artificial nanostructures have emerged as an appealing alternative for the construction and study of chirality, which have attracted tremendous interest due to the endless possibilities they provide for the real applications of chirality in biosensing, chemistry, and spin nanophotonics.[4–6] With the advantages of arbitrary design of structural symmetry and effective enhancement of the light–matter interaction, artificial nanostructures have phenomenal chiral optical responses compared to those of natural molecules. Both intrinsic and extrinsic chiral optical responses of artificial nanostructures have attracted significant attention among the scientific community.[7–37] Recent advances further validated that the chiral optical responses of artificial nanostructures can be dynamically modulated.[38,39] The intrinsic chiral optical response is associated with structural chirality under normal incidence of light, while the extrinsic chiral optical response is derived from structural anisotropy of planar nanostructures or oblique incidence of light.[2,40,41] The implementation of intrinsic chiral optical response in artificial nanostructures always involves few-layer designs or three-dimensional complex structures to break the structural mirror-reflection symmetry.[24–30] For example, a diatomic metallic nanostructure composed of a twisted vertical split-ring resonator and a wall was recently proposed to realize high-Q resonances with strong circular dichroism.[30] These approaches have high

requirements on sample fabrication tolerance and structural interlayer alignment, challenging the sample fabrication technology.

The development of hybrid bilayer plasmonic metasurfaces has proven that they have some advantages in meeting this challenge. The hybrid bilayer plasmonic metasurfaces, which can be simply fabricated via a facile one-step nanofabrication process, are composed of metallic nanostructures and their Babinet-inverted apertures in a metallic film.[42–44] Compared with previous few-layer metasurfaces, this kind of design can involve a strong near-field coupling effect without concern about layer alignment when interacting with optical waves.[45–47] Thus, hybrid bilayer plasmonic metasurfaces are good alternatives for the construction and study of chirality. Studies on the chirality of hybrid bilayer plasmonic metasurfaces have yet to be presented.

Here, we analyze the intrinsic chiral optical response of a type of hybrid bilayer plasmonic metasurface. A couple of hybrid bilayer plasmonic metasurfaces with opposite structural symmetry breaking are proposed to realize LCP-selective and RCP-selective transmission of optical waves at 750.5 nm with circular dichroism in transmission (CDT) over 25%. The chiral optical responses of the proposed metasurfaces are attributed to the near-field light interference caused by strong interlayer coupling and significantly associated with the structural mirror symmetry. We further experimentally validate the opposite chiral optical responses of a couple of hybrid bilayer plasmonic metasurfaces with opposite structural mirror symmetry breaking. Meanwhile, we experimentally demonstrated the good performance of the proposed metasurfaces for chiral optical encryption, although the efficiency of CDT and the quality factor of the chiral optical response of the proposed metasurfaces are limited due to the metallic loss. These results indicate that hybrid bilayer plasmonic metasurfaces are good candidates for the implementation of intrinsic chiral optical responses, which provide important insight for further investigations of chirality in hybrid bilayer plasmonic metasurfaces.

A schematic of the designed metasurfaces is shown in Fig. 1. The proposed metasurfaces are designed on the SiO_2 substrate. The unit cell of the proposed design is composed of a gold square-shaped nanostructure and its Babinet-inverted aperture in a gold film, which are separated by a cubic pillar made of hydrogen silsesquioxane (HSQ) negative E-beam resist. The HSQ cubic pillar is designed to rotate along the z-axis with an orientation angle equal to α (angle with the y-axis). The periods of the unit cell are all $P = 450$ nm along the x- and y-directions. The length of the gold square-shaped nanostructure is $l = 260$ nm. The thickness of the gold square-shaped nanostructure and the gold film is $t_1 = 20$ nm, and the thickness of the HSQ cubic pillar is $t_2 = 60$ nm, indicating that the distance between the gold film and the gold square-shaped nanostructure is $d = 40$ nm. Chiral optical responses can be obtained in the proposed hybrid bilayer plasmonics metasurfaces, whose structural mirror symmetry is broken by changing the orientation angle α. Moreover, for designed metasurfaces with opposite orientation angles, their chiral optical responses are opposite. A giant chiral optical response and spin-selective transmission of optical waves can be realized in the proposed metasurfaces in which the orientation angle α equals 22.5° or −22.5°.

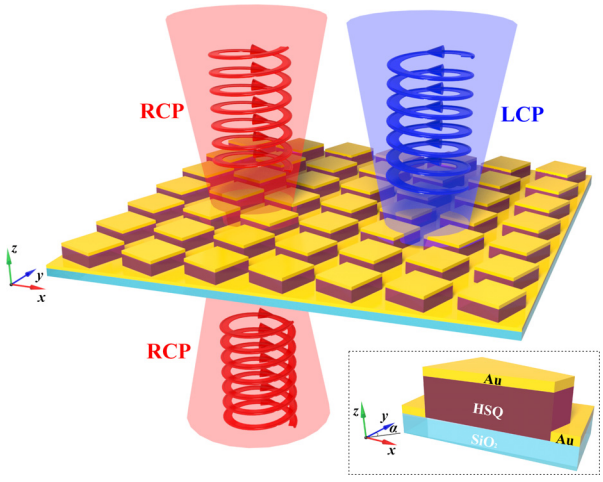

FIG. 1. Schematic of the spin-selective transmission of optical waves in the proposed hybrid bilayer plasmonic metasurface and the sectional view of its basic unit cell.

First, to validate the intrinsic chiral optical responses of the designed metasurfaces and the spin-selective transmission of optical waves, we simulated the transmission coefficients of the Jones matrix of the proposed metasurfaces under normal incidence of light. The details of the simulation method can be found in the supplementary material. Figures 2(a) and 2(b) show the simulated results of the modular square $t_{ij}=|T_{ij}|^2$ of the transmission coefficients of two designed metasurfaces with $\alpha = 22.5°$ and $-22.5°$. The subscripts "i" and "j" indicate the polarization state of transmitted and incident optical waves, respectively (L represents LCP and R represents RCP). Results indicate that the modular square of the polarization-converted coefficients t_{LR} and t_{RL} is equal to zero in the interested bandwidth. Spin-selective transmission of optical waves can be observed near 750 nm since t_{LL} or t_{RR} is close to zero. The CDT is derived from the transmission difference between the polarization-preserved components t_{LL} and t_{RR}, indicating that our designs have intrinsic chiral optical responses, and the chiral optical responses of the two designed metasurfaces are opposite. The two designed metasurfaces can be treated as enantiomorphs. We also validate that the reflection spectra of the designed metasurfaces under LCP and RCP illuminations are the same (see section 2 of the supplementary material). For further illustration of the chiral optical responses of the designed metasurfaces, the calculated results of CDT defined as $\Delta = t_{LCP} - t_{RCP}$ are shown in Fig. 2(c). The results indicate that CDT has a valley value of −0.258 at 750.5 nm (P_1) for the proposed metasurface with $\alpha = 22.5°$, while CDT has a peak value of 0.258 at 750.5 nm (P_2) for the proposed metasurface with $\alpha = -22.5°$. In addition, the two designed metasurfaces have no chiral optical response at 803.0 nm (P_3).

To clearly analyze the origin of chirality in the proposed metasurfaces, we calculate and compare the scattering power of multipole excitations in the designed metasurfaces by utilizing the electromagnetic multipole expansion method.[48] The mainly contributed excitations in the designed metasurface with $\alpha = 22.5°$ under the illumination of LCP and RCP waves propagating along the $-z$ direction are shown in Figs. 3(a) and 3(b), respectively. The calculated results indicate that the main contributor to the scattering of optical waves in the proposed metasurfaces is the electric dipole. For the proposed metasurface with $\alpha = 22.5°$, the excitation of the electric dipole is enhanced under the illumination of LCP optical waves, resulting in low transmission. The spin-selective excitation of electric dipole at the resonant wavelength is

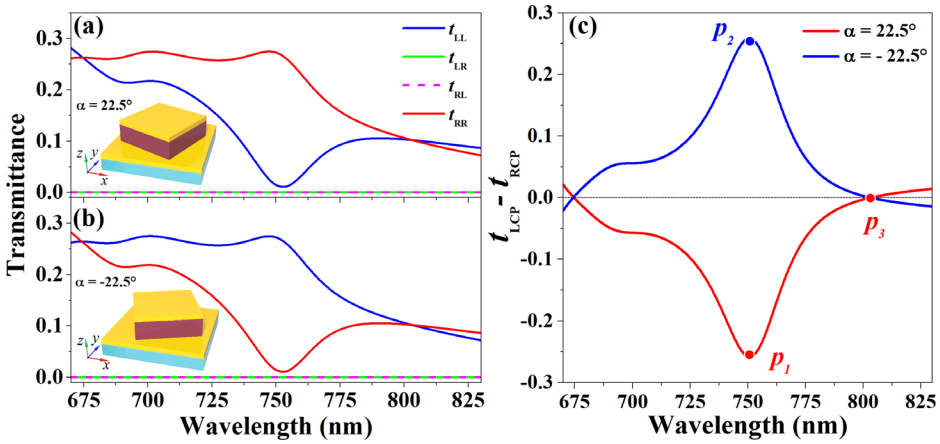

FIG. 2. Simulated results of the chiral optical responses of the proposed metasurfaces. Simulated results of $t_{ij} = |T_{ij}|^2$ with (a) $\alpha = 22.5°$ and (b) $\alpha = -22.5°$. (c) The CDT of proposed metasurfaces with $\alpha = 22.5°$ and $-22.5°$.

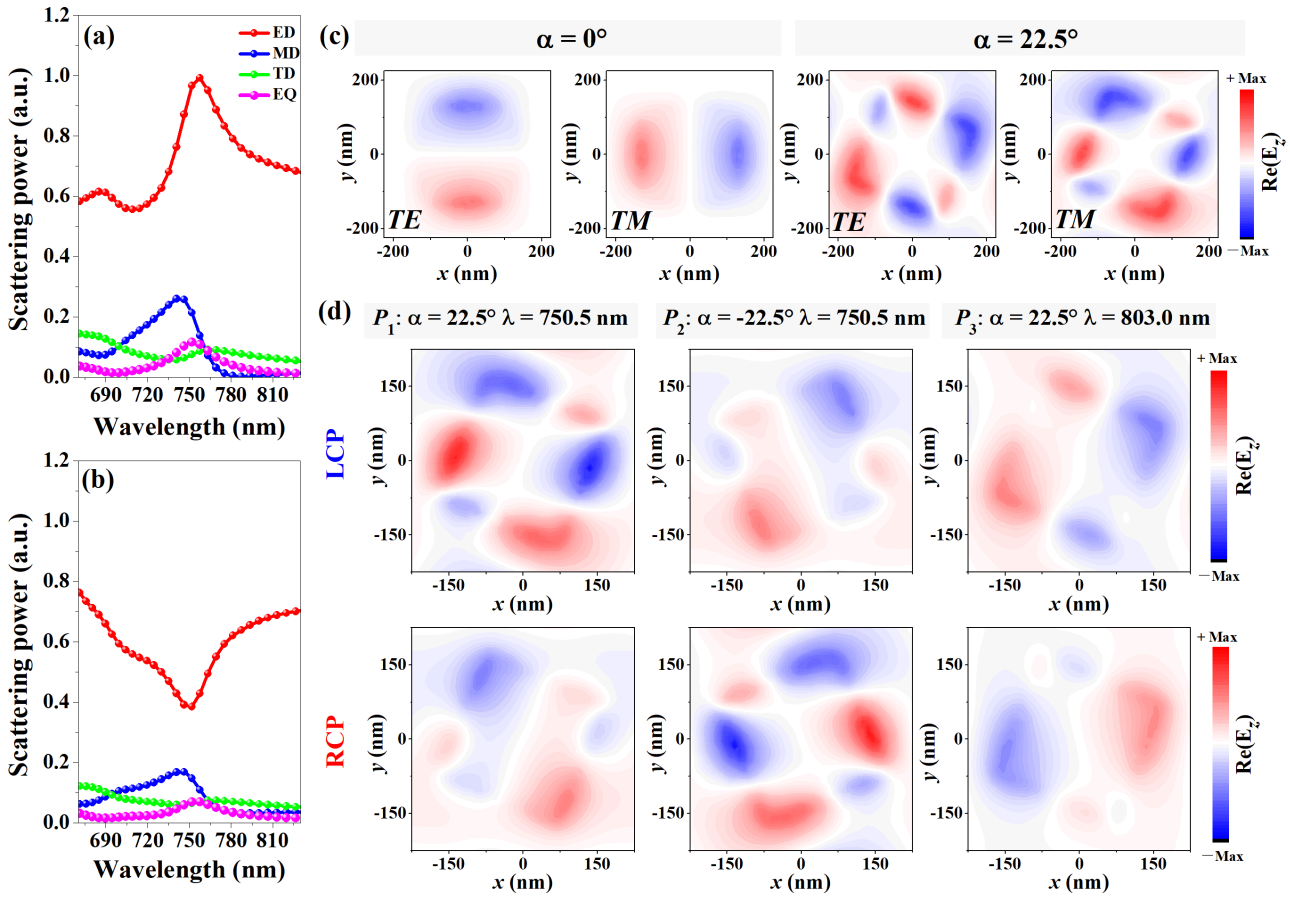

FIG. 3. The physical mechanism of chiral optical responses of the proposed metasurfaces. Calculated results of the multipolar decomposition of the scattering spectra of the proposed hybrid bilayer plasmonic metasurface with α equal to 22.5° in terms of electric dipole (ED), magnetic dipole (MD), toroidal dipole (TD), and electric quadrupole (EQ) under normal incidence of (a) LCP and (b) RCP waves. (c) The simulated distributions of the real part of the z component of electric field in the middle cross section of the unit cell (20 nm from the gold film along the $+z$ direction) under normal incidence of x- and y-polarized (TM and TE) waves at 750.5 nm for the metasurface with $\alpha = 0°$ and 22.5°, respectively. (d) The simulated distributions of the real part of the z component of electric field in the middle cross section of the unit cells under normal incidence of LCP and RCP waves at P_1 for the metasurface with α equal to 22.5°, P_2 for the metasurface with α equal to $-22.5°$, and P_3 for the metasurface with α equal to 22.5°.

attributed to the near-field light interference caused by strong interlayer coupling. As shown in Fig. 3(c), two resonant modes caused by strong interlayer coupling can be excited under normal incidence of x- and y-polarized waves when $\alpha = 0°$. The field distributions of these two resonant modes (TE and TM modes) are identical and perpendicular to each other, resulting in negligible field interference under normal illumination of circularly polarized waves. On the contrary, the field distributions of the TE and TM modes excited under normal incidence of x- and y-polarized waves are overlapped with each other when $\alpha = 22.5°$. Since circularly polarized waves are composed of x- and y-polarized waves with $\pm\frac{\pi}{2}$ phase difference, the locally enhanced electric fields associated with the two resonant modes in the proposed metasurfaces with $\alpha = 22.5°$ can spin-selectively interfere with each other under normal illumination of circularly polarized waves. The constructive and destructive interference of local electric fields can be realized by properly adjusting the structural parameters, resulting in spin-selective absorption enhancement. As illustrated in Fig. 3(d), the local electric fields associated with TE and TM modes constructively interfere with each other at 750.5 nm for LCP illumination while they destructively interfere with each other for RCP illumination when $\alpha = 22.5°$. The phase difference between the TE and TM modes is opposite when $\alpha = -22.5°$. Moreover, the enhancement of local electric field at 803.0 nm (P_3) does not show a spin-selective feature when $\alpha = 22.5°$, presenting a non-chiral optical response. These results clearly show that the chiral optical responses of the proposed metasurfaces are mainly attributed to the spin-selective collective interference of locally enhanced electric fields excited by the x- and y-components of the circularly polarized waves.

Since the field interference between TE and TM modes can be effectively manipulated by changing the orientation angle α, the intrinsic chiral optical response of the proposed metasurface can be easily adjusted. To make a further validation, we analyze the influence of the orientation angle α on the chiral optical response of the proposed metasurface. The simulated results of the variation of the transmission spectra and the corresponding calculated CDT with the change of the orientation angle α are shown in Fig. 4. The results indicate that the value of CDT and the corresponding response wavelength are significantly manipulated by the orientation angle α of the proposed metasurfaces. For the proposed metasurfaces with orientation angles α equal to -45, 0, and 45 degrees, the value of CDT is equal to zero, which demonstrates the inexistence of chirality. Moreover, opposite chiral optical responses can be realized by involving opposite structural mirror symmetry breaking. We also analyze the influence of the structural parameter variation of the proposed metasurface on its chiral optical response (see section 3 of the supplementary material). The results indicate that the thickness of the gold film has a significant influence on the CDT of the proposed metasurfaces. It is reasonable since the resonance of the gold square-shaped nanostructure and its Babinet-inverted aperture in a gold film change significantly with the increase in their thickness, resulting in the variation of the interlayer coupling. Similarly, if the sidewall of the HSQ cubic pillar is coated by a thin gold film, the interlayer coupling in the proposed metasurfaces will change, resulting in the disappearance of intrinsic chiral optical response at 750.5 nm.

To experimentally validate the chiral optical responses of the hybrid bilayer plasmonics metasurfaces, we designed and fabricated hybrid bilayer plasmonic metasurfaces with orientation angles α equal to 22.5° and −22.5°, as shown in Figs. 5(a) and 5(b), respectively. Details of the sample fabrication process and experimental setups can be found in sections 4 and 5 of the supplementary material. The measured transmission spectra of the fabricated metasurfaces under LCP and RCP illuminations are shown in Figs. 5(c) and 5(d). The slight difference between the measured transmission spectra under LCP and RCP illuminations can be attributed to sample fabrication imperfections and the subtle change of the relative angles of the samples to the incident light under different measurements. Results validate the existence of chiral optical response, and the measured results are in reasonable agreement with the simulated results in Fig. 2. Further analysis indicates that an extra thin (3 nm) chromium (Cr) film that has been added in the fabrication process as an adhesive layer influences the chiral optical responses of the proposed metasurfaces. Considering the Cr film in the fabricated metasurfaces, the simulated results show good agreement with the measured results, as illustrated in Figs. 5(e) and 5(f). The CDT decreases with the increase in the thickness of the Cr film validated by the results in section 6 of the supplementary material. Note that the Cr film as the adhesive layer is not

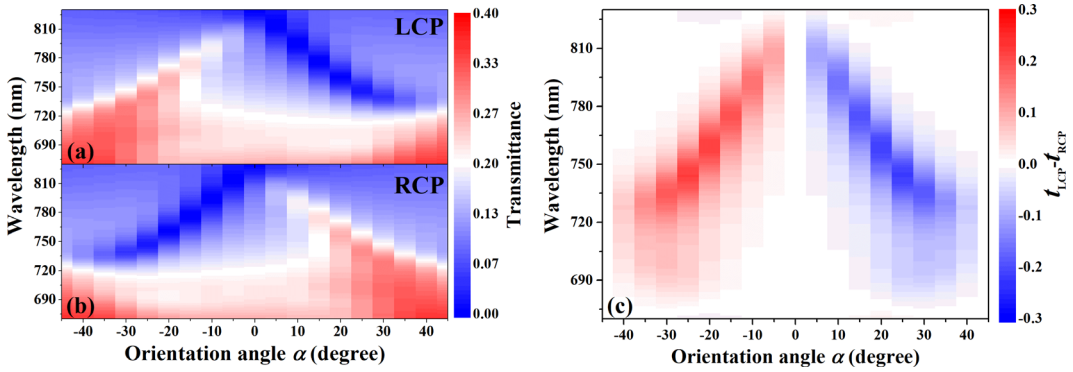

FIG. 4. The influence of the orientation angle α on the chiral optical responses of the proposed metasurfaces. The simulated results of the variation of the transmission spectrum with the change of the orientation angle α under the illumination of (a) LCP and (b) RCP waves. (c) The simulated results of the variation of the CDT with the change of the orientation angle α.

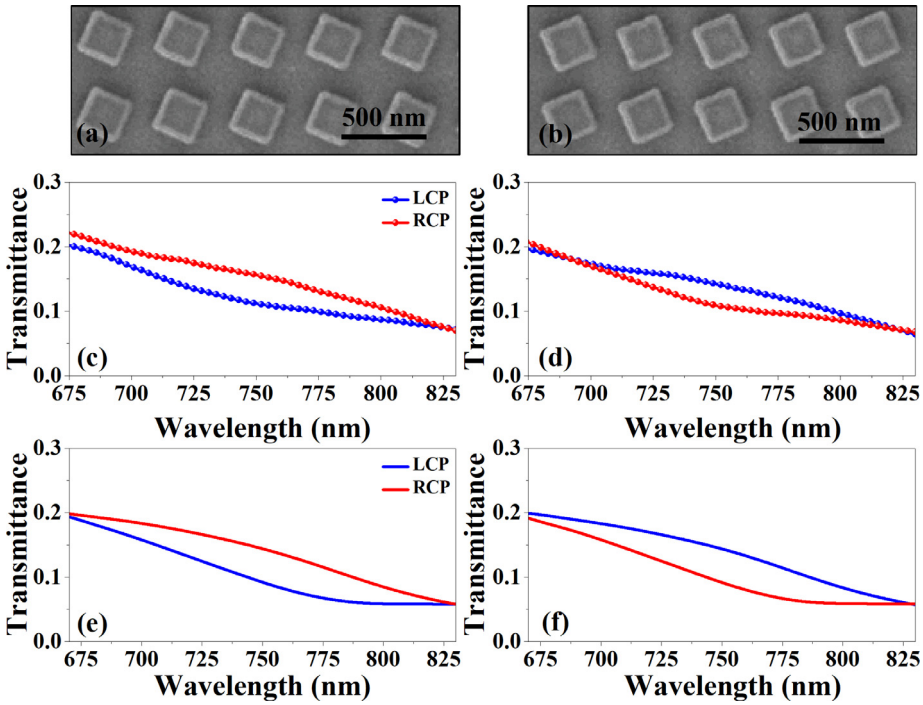

FIG. 5. Experimentally measured results of the chiral optical responses of the proposed hybrid bilayer plasmonic metasurfaces. Scanning electron microscopy (SEM) images of the proposed hybrid bilayer plasmonic metasurfaces with α equal to (a) 22.5° and (b) −22.5°. The measured transmission spectra for hybrid bilayer plasmonic metasurfaces with α equal to (c) 22.5° and (d) −22.5°. The simulated results of the transmission spectra for hybrid bilayer plasmonic metasurfaces with α equal to (e) 22.5° and (f) −22.5°, with the consideration of the extra thin Cr film added in the fabrication process.

necessary for the fabrication of hybrid bilayer plasmonic metasurfaces, but it is difficult for us to fabricate this kind of sample due to our limited processing technology.[29]

The proposed metasurfaces can be widely used in spin photonics. As an example, we demonstrate spin-selective optical encryption by utilizing the chiral optical responses of the fabricated metasurfaces, as shown in Fig. 6. Figure 6(a) shows a schematic of the designed encoded image. The designed encoded image has 50 × 50 pixels. As shown in Fig. 6(b), each pixel consists of 4 × 4 unit cells with structural orientation angles α equal to 22.5° or −22.5°. Figure 6(c) shows the captured image of the encoded image under the illumination of a broadband source (a tungsten lamp), 750 nm LCP, RCP, and linear-polarized laser source. The fabricated metasurfaces show negligible chiral optical response in the visible spectrum, and the transmission intensities of all unit cells are the same under the illumination of natural light, which results in a natural hiding of the encoded image when under the illumination of natural light. The encoded image can be decrypted only under the illumination of LCP or RCP waves near 750 nm. These results indicate that the spin-selective optical encryption we demonstrated effectively hides the information.

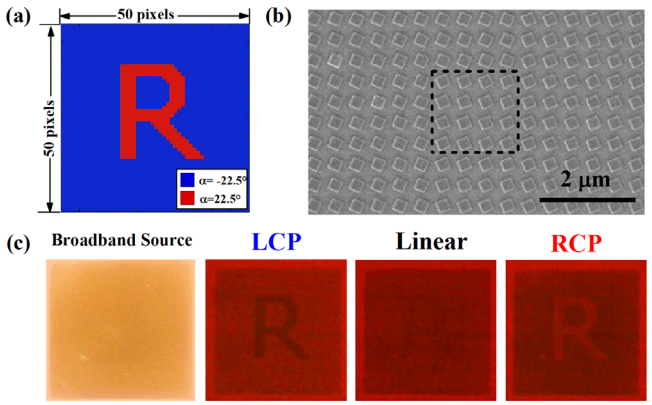

FIG. 6. The implementation of optical encryption by utilizing the chiral optical responses of the proposed hybrid bilayer plasmonic metasurfaces. (a) Schematic of the designed encoded image. (b) SEM image of the fabricated encoded image. The area inside the black boundary is one pixel. (c) The experimental results of the encoded image under the illumination of a broadband source (a tungsten lamp), 750 nm LCP, RCP, and linear-polarized laser source.

In conclusion, we analyze the origin of intrinsic chiral optical responses of the proposed hybrid bilayer plasmonic metasurfaces. The intrinsic chiral optical responses of the proposed metasurfaces are significantly associated with the structural mirror symmetry. We demonstrate that breaking the structural mirror symmetry of the proposed metasurfaces leads to spin-selective collective interference of locally enhanced electric fields excited by the x- and y-components of the circularly polarized waves, resulting in CDT. Two hybrid bilayer plasmonic metasurfaces with opposite symmetry breaking are designed to realize spin-selective transmission of optical waves at 750.5 nm with CDT over 25%. We further experimentally validate the opposite chiral optical responses in a couple of hybrid bilayer plasmonic metasurfaces and prove that the proposed metasurfaces can be used for optical encryption. Compared with few-layer designs or three-dimensional complex structures, the proposed metasurfaces fabricated via a facile one-step nanofabrication process provide a powerful candidate for the realization of intrinsic chiral optical response in plasmonic nanostructures, which can be further used for the implementation of chiral optical encryption and sensing.

See the supplementary material for more information about the details of the simulation method, the reflection and absorption spectra of the designed metasurfaces, the affection of structural parameters on the CDT of the proposed metasurfaces, the sample fabrication process, the details of experimental setups, and the affection of the thickness of the Cr film on the CDT of the designed metasurfaces.

This work was supported by the National Key Research and Development Program of China (Nos. 2021YFA1400601 and 2022YFA1404501), the National Natural Science Fund for Distinguished Young Scholars (No. 11925403), the National Natural Science Foundation of China (Nos. 12122406, 12192253, 11974193, 12274237, 12274239, and U22A20258), and the Natural Science Foundation of Tianjin (Nos. 22JCYBJC01350, 22JCZDJC00400 and 22JCYBJC00800).

AUTHOR DECLARATIONS

Conflict of Interest

The authors have no conflicts to disclose.

Author Contributions

Zhancheng Li and Yifan Jiang contributed equally to this work.

Zhancheng Li: Conceptualization (lead); Data curation (lead); Formal analysis (equal); Investigation (equal); Writing – original draft (lead). **Yifan Jiang:** Formal analysis (equal); Investigation (equal); Visualization (equal). **Wenwei Liu:** Investigation (supporting); Validation (equal). **Yuebian Zhang:** Investigation (supporting); Validation (lead). **Hua Cheng:** Formal analysis (equal); Supervision (equal); Writing – review & editing (supporting). **Junjie Li:** Data curation (supporting); Supervision (equal); Writing – review & editing (equal). **Jianguo Tian:** Formal analysis (equal); Supervision (equal). **Shuqi Chen:** Project administration (equal); Supervision (equal); Writing – review & editing (equal).

DATA AVAILABILITY

The data that support the findings of this study are available from the corresponding authors upon reasonable request.

REFERENCES

[1]A. Lininger, G. Palermo, A. Guglielmelli, G. Nicoletta, M. Goel, M. Hinczewski, and G. Strangi, Adv. Mater. **34**, 2107325 (2022).
[2]J. Mun, M. Kim, Y. Yang, T. Badloe, J. Ni, Y. Chen, C.-W. Qiu, and J. Rho, Light **9**, 139 (2020).
[3]X. Zhao, Z. Li, J. Cheng, W. Liu, S. Yu, Y. Zhang, H. Cheng, J. Tian, and S. Chen, Opt. Lett. **47**, 4814–4817 (2022).
[4]M. Qiu, L. Zhang, Z. Tang, W. Jin, C. W. Qiu, and D. Y. Lei, Adv. Funct. Mater. **28**, 1803147 (2018).
[5]Y. Chen, W. Du, Q. Zhang, O. Ávalos-Ovando, J. Wu, Q. H. Xu, N. Liu, H. Okamoto, A. O. Govorov, Q. Xiong, and C. W. Qiu, Nat. Rev. Phys. **4**, 113–124 (2021).
[6]Y. Luo, C. Chi, M. Jiang, R. Li, S. Zu, Y. Li, and Z. Fang, Adv. Opt. Mater. **5**, 1700040 (2017).
[7]J. K. Gansel, M. Thiel, M. S. Rill, M. Decker, K. Bade, V. Saile, G. Freymann, S. Linden, and M. Wegener, Science **325**, 1513–1515 (2009).
[8]M. Hentschel, M. Schäferling, T. Weiss, N. Liu, and H. Giessen, Nano Lett. **12**, 2542–2547 (2012).
[9]M. Hentschel, M. Schäferling, B. Metzger, and H. Giessen, Nano Lett. **13**, 600–606 (2013).
[10]Y. Hu, S. Xie, C. Bai, W. Shen, and J. Yang, Crystals **12**, 1052 (2022).
[11]Y. Cui, L. Kang, S. Lan, S. Rodrigues, and W. Cai, Nano Lett. **14**, 1021–1025 (2014).
[12]V. E. Ferry, M. Hentschel, and A. P. Alivisatos, Nano Lett. **15**, 8336–8341 (2015).
[13]X. Duan, S. Yue, and N. Liu, Nanoscale **7**, 17237–17243 (2015).
[14]A. Y. Zhu, W. T. Chen, A. Zaidi, Y. W. Huang, M. Khorasaninejad, V. Sanjeev, C.-W. Qiu, and F. Capasso, Light **7**, 17158 (2017).
[15]T. Cao, Y. Li, C. W. Wei, and Y. M. Qiu, Opt. Express **25**, 9911–9925 (2017).
[16]Y. Chen, J. Gao, and X. Yang, Nano Lett. **18**, 520–527 (2018).
[17]W. Li, Z. J. Coppens, L. V. Besteiro, W. Wang, A. O. Govorov, and J. Valentine, Nat. Commun. **6**, 8379 (2015).
[18]A. B. Khanikaev, N. Arju, Z. Fan, D. Purtseladze, F. Lu, J. Lee, P. Sarriugarte, M. Schnell, M. Schnell, M. A. Belkin, and G. Shvets, Nat. Commun. **7**, 12045 (2016).
[19]Z. Wu and Y. Zheng, Adv. Opt. Mater. **5**, 1700034 (2017).
[20]Z. Wang, L. Jing, K. Yao, Y. Yang, B. Zheng, C. M. Soukoulis, H. Chen, and Y. Liu, Adv. Mater. **29**, 1700412 (2017).
[21]Z. Li, W. Liu, H. Cheng, J. Liu, S. Chen, and J. Tian, Sci. Rep. **6**, 35485 (2016).
[22]S. Fasold, S. Linß, T. Kawde, M. Falkner, M. Decker, T. Pertsch, and I. Staude, ACS Photonics **5**, 1773–1778 (2018).
[23]S. Yang, Z. Liu, S. Hu, A. Z. Jin, H. Yang, S. Zhang, J. Li, and C. Gu, Nano Lett. **19**, 3432–3439 (2019).
[24]Y. Zhao, M. A. Belkin, and A. Alù, Nat. Commun. **3**, 870 (2012).
[25]S. P. Rodrigues, Y. Cui, S. Lan, L. Kang, and W. Cai, Adv. Mater. **27**, 1124–1130 (2015).
[26]Z. Li, W. Liu, H. Cheng, S. Chen, and J. Tian, Sci. Rep. **7**, 8204 (2017).
[27]C. Y. Ji, S. Chen, Y. Han, X. Liu, J. Liu, J. Li, and Y. Yao, Nano Lett. **21**, 6828–6834 (2021).
[28]I. Sakellari, X. Yin, M. L. Nesterov, K. Terzaki, A. Xomalis, and M. Farsari, Adv. Opt. Mater. **5**, 1700200 (2017).
[29]Y. Liang, H. Lin, K. Koshelev, F. Zhang, Y. Yang, J. Wu, Y. Kivshar, and B. Jia, Nano Lett. **21**, 1090–1095 (2021).
[30]Y. Tang, Y. Liang, J. Yao, M. K. Chen, S. Lin, Z. Wang, J. Zhang, X. G. Huang, C. Yu, and D. P. Tsai, Laser Photonics Rev. **17**, 2200597 (2023).
[31]A. Movsesyan, L. V. Besteiro, X. T. Kong, Z. Wang, and A. O. Govorov, Adv. Opt. Mater. **10**, 2101943 (2022).
[32]Z. Cheng and M. R. Jones, Nat. Commun. **13**, 4207 (2022).
[33]Y. Cheng, F. Chen, and H. Luo, Phys. Lett. A **384**, 126398 (2020).
[34]J. Fan and Y. Cheng, J. Phys. D **53**, 025109 (2020).
[35]Y. Cheng, F. Chen, and H. Luo, Nanoscale Res. Lett. **16**, 12 (2021).
[36]Z. Shen, S. Fan, W. Yin, S. Li, Y. Xu, L. Zhang, and X. Chen, Laser Photonics Rev. **16**, 2200370 (2022).
[37]F. Xie, M. Ren, W. Wu, W. Cai, and J. Xu, Appl. Phys. Lett. **122**, 071701 (2023).
[38]S. Dong, Q. Hu, W. Yang, K. Qu, K. Chen, T. Jiang, and Y. Feng, Appl. Phys. Lett. **121**, 191701 (2022).
[39]P. T. Probst, M. Mayer, V. Gupta, A. M. Steiner, Z. Zhou, G. K. Auernhammer, T. A. F. König, and A. Fery, Nat. Mater. **20**, 1024–1028 (2021).
[40]Y. Chen, H. Deng, X. Sha, W. Chen, R. Wang, Y. H. Chen, D. Wu, J. Chu, Y. S. Kivshar, S. Xiao, and C. W. Qiu, Nature **613**, 474–478 (2023).
[41]E. Plum, X. X. Liu, V. A. Fedotov, Y. Chen, D. P. Tsai, and N. I. Zheludev, Phys. Rev. Lett. **102**, 113902 (2009).
[42]F. Qin, L. Ding, L. Zhang, F. Monticone, C. C. Chum, J. Deng, S. Mei, Y. Li, J. Teng, M. Hong, S. Zhang, A. Alù, and S. Zhang, Sci. Adv. **2**, e1501168 (2016).
[43]L. Huang, C. C. Chang, B. Zeng, J. Nogan, S. N. Luo, A. J. Taylor, A. K. Azad, and H. T. Chen, ACS Photonics **4**, 2111–2116 (2017).
[44]J. S. Clausen, E. Højlund-Nielsen, A. B. Christiansen, S. Yazdi, M. Grajower, H. Taha, U. Levy, A. Kristensen, and N. A. Mortensen, Nano Lett. **14**, 4499–4504 (2014).
[45]H. Cheng, Z. Liu, S. Chen, and J. Tian, Adv. Mater. **27**, 5410–5421 (2015).
[46]S. Chen, Z. Li, W. Liu, H. Cheng, and J. Tian, Adv. Mater. **31**, 1802458 (2019).
[47]S. Chen, Y. Zhang, Z. Li, H. Cheng, and J. Tian, Adv. Opt. Mater. **7**, 1801477 (2019).
[48]P. C. Wu, C. Y. Liao, V. Savinov, T. L. Chung, W. T. Chen, Y. W. Huang, P. R. Wu, Y.-H. Chen, A.-Q. Liu, N. I. Zheludev, and D. P. Tsai, ACS Nano **12**, 1920–1927 (2018).